ELSEVIER

Contents lists available at ScienceDirect

Composites Part A

journal homepage: www.elsevier.com/locate/compositesa





Reactive extrusion additive manufacturing of a short carbon fiber thermosetting composite via active mixing

Pratik Koirala ^{a,1}, Robert Pavlovic ^{a,1}, Athena Aber ^b, Michael J. Fogg ^a, Cole Mensch ^a, Carolyn C. Seepersad ^{a,d}, Mehran Tehrani ^{a,b,c,*}

- ^a Walker Department of Mechanical Engineering, The University of Texas at Austin, Austin, TX, USA
- ^b Department of Structural Engineering, University of California San Diego, La Jolla, CA, USA
- ^c Program in Materials Science and Engineering, University of California San Diego, La Jolla, CA, USA
- ^d G.W. Woodruff School of Mechanical Engineering, Georgia Institute of Technology, Atlanta, GA, USA

ARTICLE INFO

Keywords: Active mixing Reactive extrusion Thermoset Carbon fiber Short fiber Additive manufacturing 3D printing

ABSTRACT

Reactive extrusion additive manufacturing (REAM) is a recently developed process that utilizes reactive thermoset resin-hardener systems that are mixed inside a shearing element, deposited layer by layer to form a structure, and cured in-situ without external energy. An externally powered active mixing element was developed and used to demonstrate REAM with a highly viscous resin that was filled with 10 wt% chopped carbon fibers. This was achieved by adding fumed silica and increasing the temperature of the fiber-resin mixture to enable effective in-situ mixing while maintaining shape retention upon deposition. Tensile properties of fiber-reinforced and reference REAM parts were measured and explained using their fiber alignment and length distribution. Finally, a mechanics model was utilized to determine the optimal fiber content for strength and stiffness, considering the degradation of fiber length at higher volume fractions due to the mixing.

1. Introduction

Additive manufacturing (AM) of thermosetting polymers and composites is gaining increasing interest due to their mechanical properties and thermal stability [1,2]. AM with thermosetting polymers and composites can potentially resolve many of the shortcomings of AM thermoplastics, such as slow fabrication speeds, high energy input requirements, and poor interlayer bonding [1,3,4]. Among various AM techniques amenable to thermosets, extrusion-based AM is a popular and convenient process for the fabrication of fiber reinforced polymer (FRP) composites in both continuous and chopped forms [2,3,5].

Reactive extrusion additive manufacturing (REAM) is a emerging extrusion-based AM process where resin (with or without filler) and hardener (curing agent) from two separate reservoirs are pumped and mixed directly inside the mixing element at a specified ratio, then deposited onto a print bed. REAM utilizes highly reactive resin systems, which generate a significant amount of heat capable of curing the printed part without the need for external energy. It also uses the transient rheological behavior of feedstock resin/hardener to maintain

shape immediately after extrusion [4–9]. Unlike direct ink write (DIW), however, REAM also utilizes rapid, spontaneous resin gelling to retain the shape of printed layers [10,11]. In other words, rheology stabilizes each layer immediately after deposition, while gelation stabilizes the lower layers as successive layers are added. REAM features high deposition rates and is applicable to both small- and large-scale AM with little to no external heat required for curing [6,10–12]. A requirement of REAM is to thoroughly mix the hardener and resin inside the mixing element. While fast gelling/curing is required for shape retention in REAM, it limits the time resin and hardener can spend inside the mixing element before curing and clogging the system. Passive mixers have been successfully used for REAM. These mixers are typically long to achieve sufficient mixing, yet require high extrusion rates to prevent clogging [4].

The two AM methods most similar to REAM are post-cured DIW and frontal polymerization AM [1]. Externally cured DIW is the more traditional method of extruding thermosets, in which inks are deposited on the build plate with the expectation that there will be little to no ambient curing. Curing may be accomplished by postprocessing in an

^{*} Corresponding author at: Department of Structural Engineering, University of California San Diego, La Jolla, CA, USA. *E-mail address*: tehrani@ucsd.edu (M. Tehrani).

¹ Equal contribution.

oven or by exposing layers to external energy after they have been printed, such as UV curing or radio-frequency heating [13–15]. One limitation to this method is the structural stability of the printed inks, which becomes an issue when printing larger parts. By contrast to DIW, frontal polymerization AM relies on a self-propagating reaction similar to REAM; slow curing resin and hardener are mixed, with small amounts of an initiator included to begin the reaction [14,15]. The reaction forms a 'cure front,' travelling through the deposited ink, completely (or near completely) curing material. If the deposited material is synchronized with the cure front, gravity-induced sagging is unlikely.

Inter-layer bonding must be carefully monitored in REAM parts since each layer is quickly cured right after deposition. REAM can be considered a specific form of frontal polymerization but with no need for an additional initiator/inhibitor and higher targeted deposition rates. There are two size limitations specific to REAM and frontal polymerization. For small parts that have a high surface area to volume ratio, convective heat transfer may outpace heat generation, leading to a low degree of cure near the surface. For large parts that have a low surface area to volume ratio, heat generation may outpace convective heat transfer, which may thermally decompose interior regions. Both REAM and frontal polymerization systems have been adapted for printing composites [5,16].

Within continuous-flow processes, there are two general types of mixers: active and passive. Passive mixers, which consist of unpowered rotating or static elements that encourage folding and interdigitation between the two components being mixed. The energy for mixing is supplied indirectly through a pressure head. For REAM processes with passive mixing, the print resolution and the viscosity of resins, particularly fiber filled ones, are limited due to the coupled nature of the extrusion rate, travel speed, feedstock viscosities, and mixing efficacy [8]. The mixing efficacy is dependent to flow velocity through the mixing element, which subsequently influences the range of geometric fidelity and travel speeds achievable [4]. Additionally, including carbon fibers or nanoparticles to improve properties or impart functionalities increases the viscosity of resins considerably [17–20]. Altough passive mixing is a well-established and highly economical process, it is not suitable for mixing of high viscosity fluids. While more complex passive mixers are available, active mixers provide more freedom in terms of mixer compactness, range of fluid viscosities, and deposition rates by decoupling each of these sets of parameters [20]. Active mixers directly provide energy for mixing through mechanical, acoustic, or other means, which also reduces difficulties that might be involved with providing enough pressure head to passively mix corrosive, abrasive, viscous, or otherwise hazardous components. Given the limitations of passive mixing and the greatly increased viscosity in fiber-filled resins, passive mixing is clearly not suitable for thermoset resins with high fiber fills. Therefore, active mixing is essential to printing high performance composites at high resolutions [18-20].

AM has introduced innovative methods to integrate short fibers into resins, enhancing the mechanical properties of polymeric parts. The content, length, and alignment of these fibers play pivotal roles in determining these properties. During the mixing of chopped fibers, the mean fiber length will continually degrade from fiber-fiber contacts and high shear flow. With a greater fiber content, there are more fiber-fiber contacts, and the resulting mean fiber length will be smaller [34]. Given that adding more fibers to a resin can degrade fiber length, it is crucial to find a balance between high-volume fractions and the integration of longer fibers [1,21]. Although models exist that capture these effects, they have not yet been applied to a composite system to ascertain the optimal fiber content for maximizing strength and stiffness [22]. This study employs a well-established model, and combines it with experimental data on fiber content versus length, to explore the relationship between properties and fiber content for AM parts.

This work details a modification of REAM technology where the passive mixer was replaced by an externally powered ('active') mixer, offering superior mixing quality by decoupling the mixing dynamics from the extrusion rate. This modification enabled greater control over process parameters, higher print resolution, and extrusion of higher viscosity feedstocks for high performance composites, while maintaining mixing quality and reliable curing.

2. Materials, manufacturing, characterization, and modelling

2.1. Materials

The epoxy resin system used in this study was EPON 8111 (Bisphenol A/TMPTA) with EPIKURE Curing Agent 3271, both sourced through Hexion Inc. When mixed, they feature a low viscosity and a short gel time of approximately 60 s [4]. The chopped carbon fibers used in this study (\sim 7µm diameter, up to 3 mm long) came with sizing for epoxy resins. Fibers were pre-mixed in a 1:9 wt ratio to resin/curing agent, yielding an overall 10 wt% fiber fraction, equivalent to 6.7 vol%. Fiber fractions of 20, 30, and 40 wt% were attempted, but could not be successfully printed due to fiber settlement, aggregation, and clogging during the initial heating and degassing steps. To achieve sufficient shear yield strength for retaining the shape of the extrudate after it exits the mixing element nozzle, 2.5 wt% of fumed silica (CAS 112945–52-5 Sigma Aldrich, 5–50 nm in length and surface area of 50–600 m²/g) was also pre-mixed in the fiber polymer mixture as a rheological modifier.

A 2-liter, epoxy/carbon fiber/fumed silica formulation was created and pre-mixed for 18 h (which was later found to be far too long) with a shear mixer (IKA RW 20 Digital high shear mixer) at 500RPM. Samples of this mixture were taken for viscosity and fiber length measurements. The mixture was transferred to a reservoir, degassed at -30 inHg for 1 h, and heated until the surface temperature of the mixture reached 70 $^{\circ}$ C. This preheat treatment was introduced to reduce the material viscosity, which would improve degassing and hamper clogging during REAM. The hardener agent was treated similarly, being pre-mixed with the same shear mixer and 3.5 wt% fumed silica, then degassed at -30 inHg for 1 h.

2.2. Additive manufacturing

The reactive extrusion additive manufacturing (REAM) system was described comprehensively in Uitz et al. [8[x with an overview provided here. The REAM system included metering and positioning subsystems. The metering system used progressive cavity pumps (Netzsch NDP-1000-03 and NDP-800-03) to draw precursors-resin and hardener—from separate reservoirs into a mix manifold at a prescribed ratio. The separate streams of resin and hardener combined when they exited the mix manifold and entered an extrusion assembly, which included either a passive or an active mixer. The mixing element combined the precursors together, which triggered a polymerization reaction that continued after the material exited the mixing element, through a nozzle, and onto the build envelope. The extrusion assembly was coupled to the positioning system—specifically, the end-effector of a 6 degree of freedom robotic arm (Yaskawa Motoman, MH80)-which controlled the motion of the nozzle. Custom software was used to convert a g-code file generated by a fused filament fabrication (FFF) path planning algorithm into a robotic trajectory. The robot trajectory was executed and synchronized with pumping using ROS (Robot Operating System). A depiction of the system is shown in Fig. 1.

As illustrated in Fig. 2, the design of the active mixing element was inspired by previous research into active mixing of complex fluids [23]. The active mixing element comprised a cross-shaped chamber with a mixing region in the center, two material inlets on the sides, and a single outlet nozzle on the bottom. The top of the chamber transferred no material, but instead interfaced with a rotating impeller powered by a motor. The impeller spun at a constant rotational speed while material entered via the inlets, where pressure forced the material down and out of the mixer. The difference in rotational velocity between the impeller and the static mixer walls caused high shear rates, which introduced

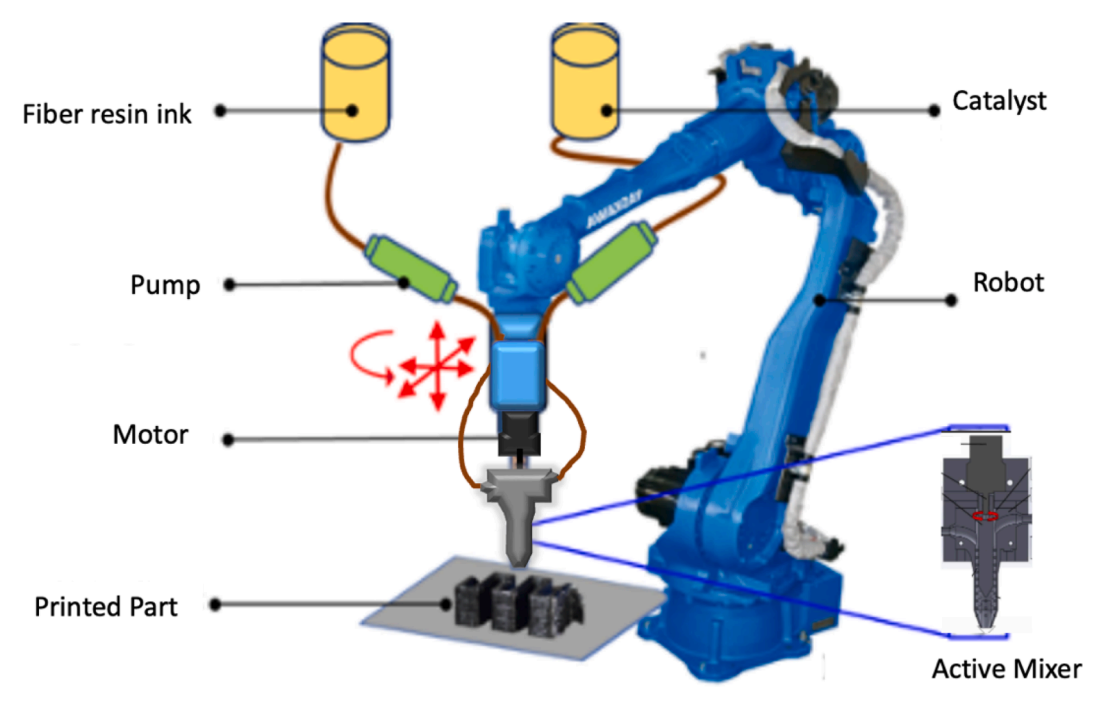


Fig. 1. A depiction of the REAM system with an active mixing element.

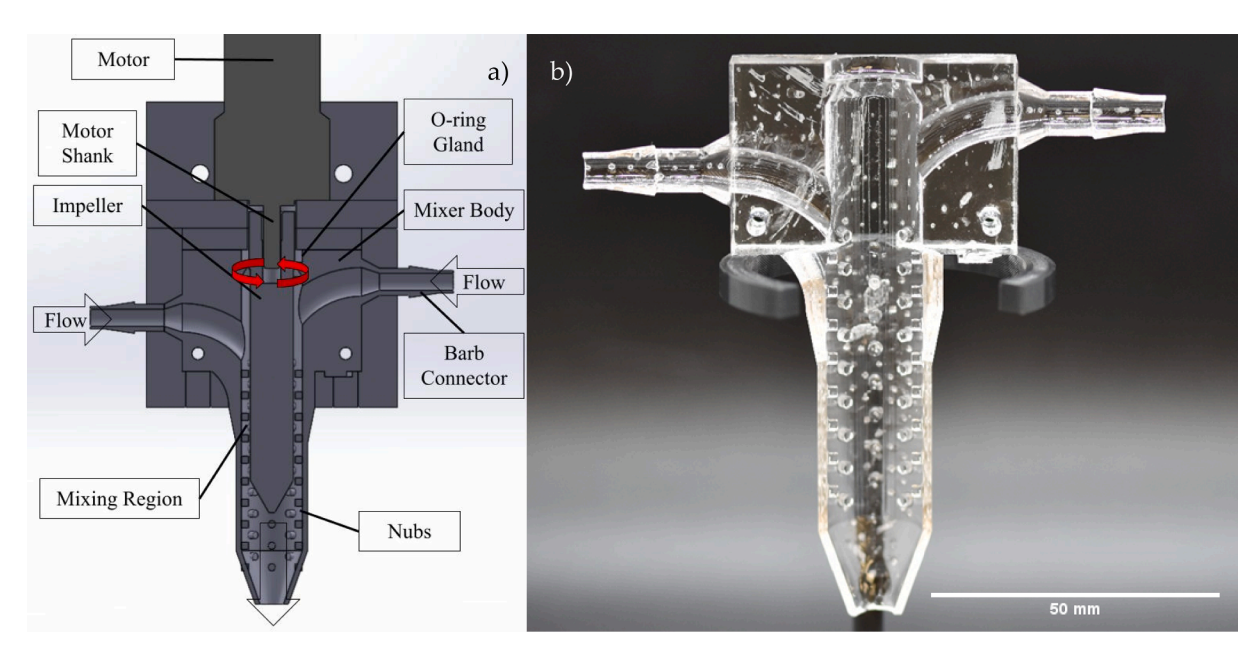


Fig. 2. a) CAD cutaway of the active mixing printhead. b) Printed cutaway of the printhead in a trasparent polymer.

new material flows and promoted mixing by interdigitation and diffusion. Adapting this design to feed viscous, fiber-loaded resins required an extensive amount of testing and redesigning, with notable changes that included mechanical reinforcement to prevent vibrations from the motor causing chatter marks, the sloping and staggering of the feed ports to reduce backflow, multiple redesigns of the dynamic seals to prevent leakage, and the addition of nubs within the mixing chamber to disperse fiber clumps and improve mixing quality.

To minimize carbon fiber clogging, the internal dimensions were selected such that the resin mixture and clumps of fibers passed through the system without clogging or gelling. The final design included a mixing chamber internal diameter of 17 mm, impeller outer diameter of 12 mm, and tip outlet diameter of 6.5 mm. The inlets initially measured at 4.75 mm, expanding to 8 mm in diameter; the smaller initial diameter

accomodated the external dimensions of the barb connectors, with the larger diameter preferred to reduce the likelihood of clogging. The geometry was tuned for a 625 RPM impeller, up to 20 mm/s print speed, and 6.5 mm diameter depositing nozzle (which corresponded to a flowrate of approximately 2,400 cm 3 /hour, or 0.67 mL/s), so that the residence time in the mixer was less than 60 s to prevent gelling [4,8].

As mentioned earlier, mixing occured through a combination of interdigitation and diffusion [20]. Interdigitation, driven by the rotating impeller, increased the surface area between the resin and hardener by creating thin alternating layers of fluids, shown in Fig. 3. The specific layer thickness depended on mixer geometry, shear rate, mixing time, and fluid properties. Diffusion between the thin layers of resin and hardener surfaces was intended to induce thorough mixing, thereby facilitating a near-complete cure [23].

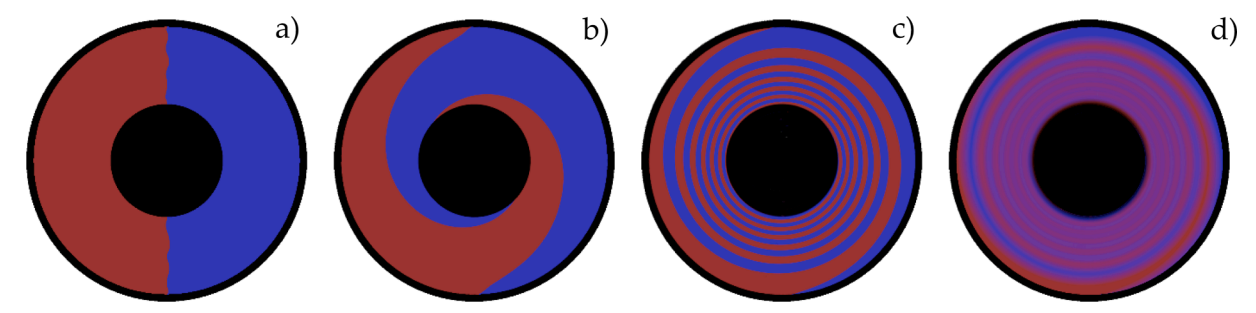


Fig. 3. a) Top-down view of the starting positions of fluids in the active mixer. b-c) Rotation of the impeller and mixing by interdigitation, where progressively thinner layers of alternating fluids were formed. d) Diffusion between layers causing complete mixing. This only applied to the mixing region, identified in Fig. 2.

The shear rate in the mixing region was calculated to be on the order of 10– $100~s^{-1}$ by assuming smooth walled geometries then unwrapping the mixer body and impeller such that they act as a set of planes in simple shear. Computational fluid dynamic analysis indicated a similar shear rate for passive mixing REAM [24]. At this rate, the shear thinning property of the resin mixture reduced the load on the motor driving the impeller.

The mixing element (both body and impeller) was manufactured by FFF 3D printing (Ender 3 Pro), using eSun PLA + at a 0.2 mm layer height and 20% infill. The O-ring gland was conventionally machined into the design and fitted for a dash 112O-ring to achieve a forgiving dynamic seal.

The REAM system was programmed to extrude a single raster with a linewidth of 6.5 mm and an individual layer height of 3 mm. The raster was deposited in an oval (racetrack) pattern with a major axis of 100 mm, a minor axis of 50 mm, and 7 layers of deposition. The material flowrate was set at $40~\rm cm^3/min$, and the material was deposited onto a heated build plate with a temperature of $60~\rm ^{\circ}C$. An attempt was made to use a passive mixer for a direct comparison of results, but this passive mixer was not able to successfully print the highly viscous ink used here due to issues identified in the introduction section [8].

2.3. Characterization

To investigate the printability of the epoxy system prior to part fabrication, scoop tests were performed to verify the formulation could retain its shape right after deposition. The tests included 20 mL of the mixed carbon fiber epoxy formulation and 5 mL of hardener to a small mixing bowl, manually mixing for 20 s (the approximate amount of time the resin and hardener would interact in the mixing chamber), and uisng a 0.5 tablespoon (7.39 ml) scoop to transfer the gelling mixture onto an aluminum tray. The printability was then assessed visually by how well it retained its shape and by the max temperature achieved during the curing process. A mixture of neat EPON 8111 mixed with 3.5 wt% fumed silica was used as a baseline for the ideal shape and peak exotherm temperature (140-160 °C) for each of these tests as it had been printed successfully in previous work [8]. To determine the dependency of viscosity on shear rate, continuous flow tests were performed at controlled shear rates from 0.01 to $100~\text{s}^{-1}$ using a TA Instruments Discovery HR-2.

To monitor fiber breakage during pre-mixing, fiber lengths were measured after the resin, fibers, and fumed silica had been pre-mixed to homogeneity. A metal spatula was used to remove samples of material from the pre-mixed formulation. These samples were then diluted with neat epoxy in a glass dish and gently mixed with the spatula to homogenize the mixture and prevent fibers from overlapping during measurement. Smaller samples were taken from this batch and spread thinly on a microscope slide, where the over 700 fibers were measured by optical microscopy (AmScope Microscope with MU1803 Digital Camera, analyzed through ImageJ). Note that this process only measures the fiber lengths of the initial mixture and does not account for potential

fiber breakdown during the printing process, although further fiber breakdown during printing is expected to be negligible compared with the rigorous shear mixing used for feedstock preparation.

Thermal footprints were acquired using a FLIR A 325 thermal camera during and after printing. Degree of cure in the REAM parts was measured using differential scanning calorimetry (DSC). Twelve total samples were taken from the part, with four samples each removed from the top, middle, and bottom. Each sample was approximately 10 mg, tested in a Netzsch DSC 214 Polyma with a pierced lid container. The DSC regimen involved a temperature ramp from 25 °C to 220 °C at a calibrated rate of 10 °C/min.

For mechanical analysis, samples were machined according to the ASTM standard D638 to create type V tensile test coupons. The coupons were cut such that the major axis of the tensile bar was parallel to the print direction, limiting interference from inter-raster effects. Given that previous work found no dependence of strength on orientation, so transverse specimens were not created [8]. The tensile specimens were loaded with a 1KN load cell on an MTS electromechanical testing device. During the test, a continuous cross head displacement rate of 1 mm/min was applied, and the strain was measured with an MTS extensometer with an 8 mm gauge length. Further details and images are available in supplementary material A. The results of these tests were then compared to a reference 3.5 wt% fumed silica filled formulation.

Fiber alignment was investigated by grinding/polishing samples and taking micrographs of the resulting surfaces (AmScope Microscope with MU1803 Digital Camera). Samples from the active mixer were polished such that faces in line to the print direction and normal to the print direction were visible. Additionally, micrographs were taken at different heights in case fiber alignment varied from layer to layer.

2.4. Modelling

An analytical model based on fiber length and orientation distribution proposed by Fu and Lauke was used to model the strength and the modulus of the REAM composite in order to find the optimal fiber volume fraction [25]. This model calculates the strength of the composite using a modified rule of mixture [26]. Further modeling details can be found in supplementary material B.

The rule of mixture may not provide accurate predictions for the elastic modulus of short fiber composites when the fibers are of varying lengths and oriented in random directions. In such cases, a laminate analogy approach can be used to calculate the composite modulus [27]. This approach takes into account both the length and orientation distribution of the fibers. It involves calculating the off-axis stress–strain relationship of the laminate for each orientation, and then integrating these values over the thickness of the material to determine the overall laminate stiffness. Further details can be found in supplementary material C.

Using the optical microscopy method described earlier, the experimental length distribution of fibers was determined. Based on this, the strength and modulus of the composite material were predicted for

various volume fractions ranging from 3 % to 35 %. The fiber orientation and length distribution were taken into account in determining the optimal amount of fiber required for optimal performance of the composite material. The parameters used for modeling are summarized in Table 1.

3. Results and discussions

3.1. Rheological properties of the ink

Understanding the rheological behavior of inks is crucial for successful REAM printing. Ideally, an ink should maintain its shape upon deposition while still permitting ease of flow in the mixing element. These characteristics typically correlate with high and low viscosities, respectively, making them challenging to achieve simultaneously. As shown in Fig. 4a, scoop tests revealed that despite its higher viscosity, a formulation with only 10 wt% carbon fibers did not retain its shape sufficiently; thus, it was not a suitable formulation for printing. Although the fibers contributed to the enhanced viscosity of the formulation, the shear yield strength and storage modulus were insufficient to preserve the shape after extrusion [28]. Scoop tests with higher fumed silica loadings (as shown in Fig. 4b-e) demonstrated that 2.5 wt% fumed silica and 10 wt% short carbon fiber are suitable for REAM printing. This means it can support its own weight and a few additional layers atop it. The necessity for rheological shape retention lasts only for tens of seconds post-deposition, as the exothermic reaction between the resin and hardener rapidly gels the material.

The viscosities of different resin formulations as a function of shear rate are documented in Fig. 5. Pure epoxy resin exhibited a Newtonian behavior with a constant viscosity of 0.8 to 1.1 Pa.s regardless of shear rate [29]. The addition of 10 wt% chopped carbon fibers (CF) increased the viscosity of the resin, but a largely shear rate independent behavior was still observed. The added fumed silica (FS) drastically increased the viscosity and shear thinning of the formulation. The fumed silica forms branching networks of flocs that greatly increase the viscosity of the host liquid but are stable only at low shear rates. High shear rates result in the breakdown of flocs, reducing viscosity [30]. Apart from improving the printability of resin, this effect means that resin in a high shear region of a mixer should exhibit reduced viscosity, which eases the task of mixing and extruding.

The static viscosity (measured at a shear rate less than $0.1~\rm s^{-1}$) of the printable carbon fiber-fumed silica resin formulation (containing 2.5 wt % fumed silica) was quite high (~300 Pa.s); however, with shear thinning the viscosity dropped to ~ 9 Pa.s at 20–80 s⁻¹ shear rates, which was comparable to the shear rates inside the mixer during printing. Raising the temperature of the carbon fiber-fumed silica resin formulation resulted in an unexpected reduction of viscosity in the 0.6–6 s⁻¹ shear rate region. This behavior helped reduce pressure heads during active mixing and facilitated mixing at lower shear rates. Higher fiber fractions were attempted, but these mixtures ultimately ran into issues with fiber settling and clogging during the degassing step.

The fabricated prints exhibited clean contours with few defects, as shown in Fig. 6. The average standard deviation of a layer width was 0.3 mm, less than $5\,\%$ of the expected raster width. This low deviation is credited to improved mixing, resulting in more gelling, faster

Table 1 Parameters used for modeling.

Parameters	Value
Fiber diameter	7 μm
Fiber tensile strength	4115 MPa
Matrix failure strength	60 MPa
Fiber tensile modulus	231 GPa
Matrix tensile modulus	3 GPa
Critical fiber length	400 μm
friction between fiber and matrix, µ	0.01

crosslinking, and less sagging after deposition. The shrinkage for these parts was not explicitly measured, but should lie around 2.1 % according to the manufacturer's technical data sheet.

3.2. Curing kinetics

Thermal videos of the REAM process were captured to gain deeper insight into the curing kinetics. Fig. 7 a-f shows a thermal timelapse of a racetrack during printing. The effect of exothermic chemical crosslinking appeared after approximately 50 s of deposition, which coincided with the deposition of the fourth layer. After approximately 4 min, the temperature reached a peak of 185 °C, at which point the majority of the curing took place. The small temperature gradients developed in the racetrack during cooling (Fig. 7 g-i) were attributed to the added carbon fiber. Carbon fibers enhanced the thermal conductivity of the polymer, resulting in a relatively uniform heat distribution. Additionally, the feedstock and bed temperatures were quite low compared with the peak exotherm (60 vs 185 °C). Curing was, therefore, driven by the exothermic heat released via the reactive resin system. Minimal part warpage was observed in the racetrack part after cooling to room temperature (see Fig. 6). This can be attributed to the uniform cooling of the whole part, reducing the development of residual stresses, and the relatively high stiffness of the part due to the carbon fiber addition.

DSC analysis was conducted on small samples taken from random regions of the racetrack. Of the twelve samples tested, two were removed as obvious outliers, resulting in the ten curves shown in Fig. 8. Partial areas of these DSC curves were evaluated and compared to the uncured control sample. Most samples displayed acceptable cure qualities (i.e., >90 %) regardless of location, with a median cure percentage of 98 % and overall average cure of 94 %. However, the standard deviation of the measurements was 6 %, due almost entirely to two tests from the bottom layer that displayed only partial curing. These tests are represented by the two partially cured samples (with peaks between 100 and 150 $^{\circ}$ C) visible in Fig. 8, which resulted in 84 % and 81 % cures. It should be noted that another base sample displayed a 97 % cure. The most likely explanation for this effect is that heat transfer from the sample to the build plate prevented full curing at the base. Thermographs shown in Fig. 7 also confirm that the bottom layers of the racetrack exhibited peak temperatures of only 100 °C, much lower than the rest of the part.

3.3. Tensile properties and structure

The tensile properties of the fiber-reinforced REAM part were compared to the baseline non-reinforced formulation with 3.5 wt% fumed silica, as shown in Fig. 9. Compared with the reference REAM sample, the 10 wt% carbon fiber samples achieved a 15 % higher strength and 55 % higher modulus in the print direction. These improvements were accompanied with a 33 % drop in failure strain, which is typical for fiber-reinforced polymers. The added carbon fibers contributed predominantly to an improvement in modulus rather than strength, which was primarily because the fibers broke down to lengths shorter than the critical fiber length when mixed into the resin, as described subsequently here.

To investigate correlations between structure and properties found above, cross-sectional microscopy was employed to reveal potential fiber alignment and identify defects created by REAM. Fig. 10 shows an inline micrograph from a REAM part where no significant difference in fiber alignment was noted across any planes. The observed round voids were likely trapped air or volatiles formed due to elevated curing temperatures. However, the void content in the fabricated sample was relatively low (<0.7 %), proving that the degassing steps effectively removed most air bubbles from the resin and hardener feedstocks.

The large nozzle size used here (i.e., 6.5 mm) was responsible for the lack of sufficient shearing of the slurry, resulting in virtually no fiber alignment. The nozzle shape used here was intended to drive high shear

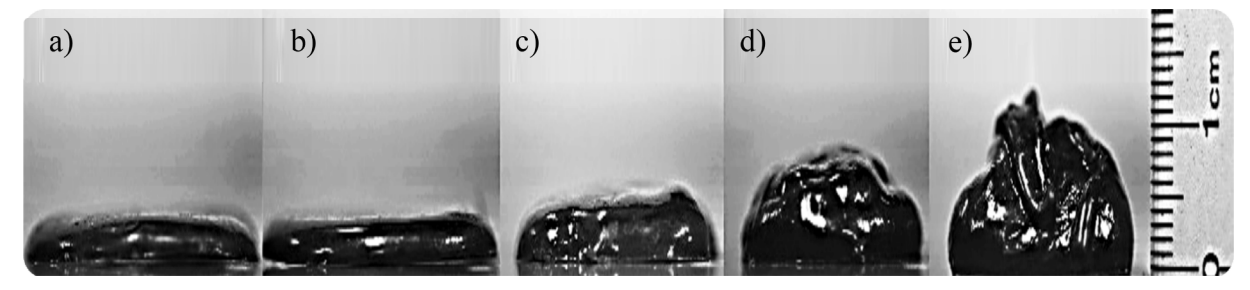


Fig. 4. Scoop test results. All tests have 10 wt% carbon fiber. Additionally, a) has no fumed silica, b) has 1 wt%, c) has 1.5 wt%, d) has 2 wt%, and e) has 2.5 wt% fumed silica.

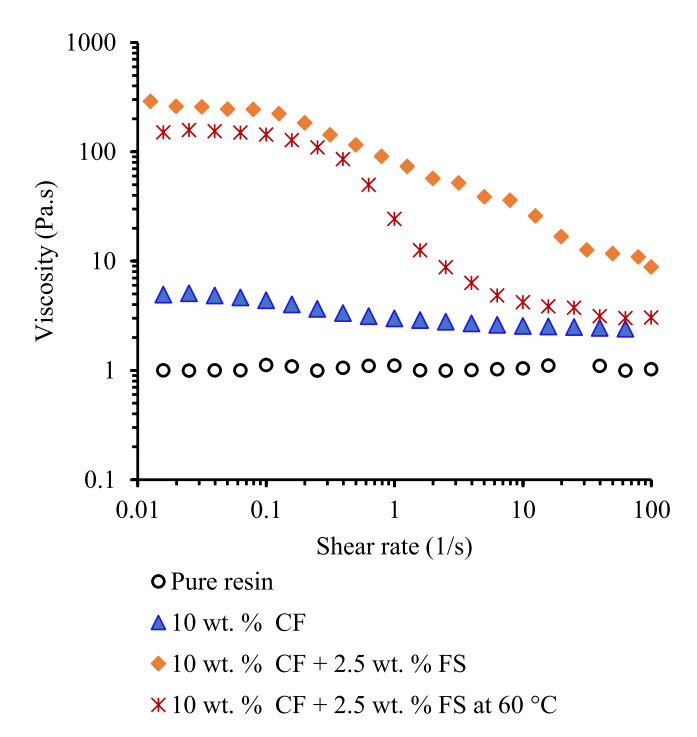


Fig. 5. Shear rate dependent viscosity of different resin formulations.

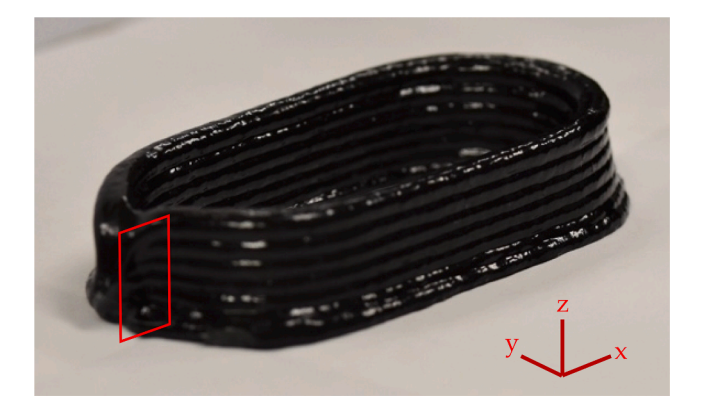


Fig. 6. Isometric view of typical racetrack prints. Racetrack axes are 10 cm by 5 cm. The red rhombus represents the location where sectioned micrographs were taken from. (For interpretation of the references to colour in this figure legend, the reader is referred to the web version of this article.)

and convergent flow, potentially aligning fibers prior to deposition [31,32]. The convergent flow was generated by the last 25 mm of travel in the mixer, where the impeller is not present, and the flow converges to the final tip diameter. It is possible that transient effects of (mis)

alignment from the rotating impeller have carried into the nozzle section, but modeling of similar (laminar) flows in FFF printers has shown little dependence of fiber alignment on the length of a convergence zone beyond five radii of the nozzle exit [32]. However, the shear and convergent flow in this nozzle design were not large enough for meaningful fiber alignment. A possible explanation is that fibers deviated from alignment in areas of low shear or divergent flow [32]. Low shear may have been present in areas far from the mixer wall or in material movement after deposition, and divergent flow may have been present in the raster deformation experienced during deposition, although the presence of fillers reduced this effect [32].

3.4. Modeling

Fiber length governs mechanical properties of resulting composite REAM parts. Fiber length distribution was, therefore, characterized in the feedstock mixture. The mixture was found to have an average fiber length of 120 μm and standard deviation of 150 μm . Fibers were unevenly distributed, with 50 % of them being less than 200 μm long, and the remainder ranging from 200 μm to 3 mm. The volume-weighted average fiber length was calculated to be 317 μm . Fig. 11a shows the fiber length probability density, displaying the nonuniform nature of fiber length distribution. It should be noted that these values are significantly different from the nominal fiber length of 3 mm observed before mixing.

Trends observed in the literature show the maximum packing of randomly mixed carbon fibers decays exponentially as their aspect ratio increases [9]. Because of this, incorporating larger fiber loadings would create a necessary reduction in fiber length (breakage) during mixing. As shown in Fig. 11b, this phenomenon has been documented in other studies, which found high fiber breakdown at the start of mixing, with the volume-weighted fiber length decreasing to a steady state value as mixing time increases [5,34]. While higher fiber fractions directly enhance many composite properties, it is also important that the fiber length exceeds the critical fiber length to facilitate effective stress transfer. Critical length of carbon fibers in thermosetting resins is $\sim 300{-}400\,\mu\text{m}$, implying most of the fibers in this study were not loaded to their strength values [35].

The tensile strength and stiffness of fiber-reinforced composites were estimated based on fiber length distributions and mechanics modeling explained earlier. These estimates were obtained by assuming several factors. First, it was assumed that fumed silica had no impact on the final density of the composite material and was thus excluded from the fiber volume fraction calculations. Additionally, all calculations were based on the fiber and matrix properties listed in Table 1, and the fiber length distribution displayed in Fig. 11a was used uniformly across all calculations. The maximum achievable volume fraction of fibers for a given length, which ensured effective packing, is depicted in Fig. 11b and was utilized in this particular study [33].

The tensile stiffness and strength of a composite reinforced with randomly aligned fibers are shown in Fig. 12a. The elastic modulus increases with increasing fiber volume fraction despite the reduction in

Composites Part A 178 (2024) 107989

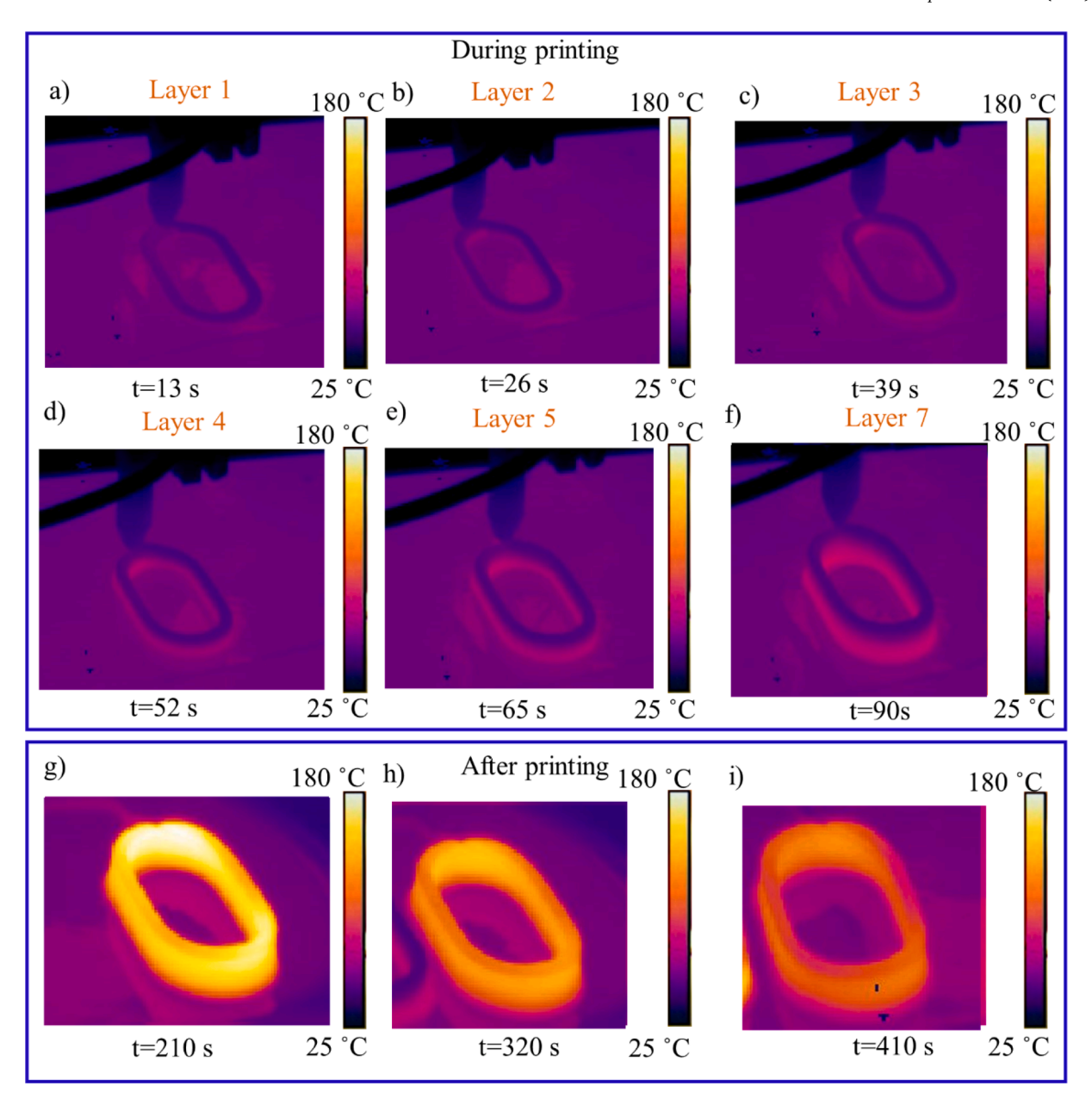


Fig. 7. Thermal images of the racetrack during and after fabrication.

fiber lengths. Fibers' contribution to the overall stiffness decreased at higher volume fractions, resulting in a concave curve shape due to the smaller aspect ratio of fibers at higher volume fractions. This effect was more pronounced for strength, as it maximized around 23 % fiber fraction, which corresponded to a fiber aspect ratio of approximately 17. Beyond this optimal volume fraction, the composite's tensile strength declined. The model appeared to overestimate the strength relative to experimental measurements. This discrepancy stemmed from the model's inability to account for stress concentration at fiber ends. In practice, other studies have found similar results for short fibers [35].

Fig. 12b presents the estimation of the tensile strength and modulus of partially aligned carbon fibers (greater than 85 %) with respect to the volume fraction of the fiber. This model assumed that fibers were predominantly aligned upon exiting the nozzle and maintained that alignment thereafter. Results suggest that fiber alignment strongly impacted the modulus, however, evident by the decreasing slop of the modulus vs volume fraction curve, reinforcement effect degraded with increasing volume fraction. Contrary to modulus, fiber alignment had no effect on the maximum achievable strength, however, it shifted the peak to lower

volume fractions; compare Fig. 12 a and b. The fact that maximum strengths were identical was largely because most fibers were shorter than the critical length required for reinforcement. The optimal volume fraction for partially aligned fibers was \sim 14 %.

4. Summary and conclusions

This paper documents the initial design and successful demonstration of an active mixing element for REAM. The system's ability to accommodate high viscosity feedstocks, even at low flow rates, made it well suited to the task of printing composites with REAM, as viscosity increases with fillers like fumed silica and carbon fiber. In this study, the inclusion of 2.5 wt% fumed silica into the fiber-resin mixture led to a notably high static viscosity and shear yield strength, essential for shape retention. At the same time, it displayed considerable thinning at higher shear rates and increased temperatures, which was crucial for in-situ mixing.

Printing at lower extrusion rates, enabled by active mixing, allowed for more material gelling before deposition, which resulted in deposited

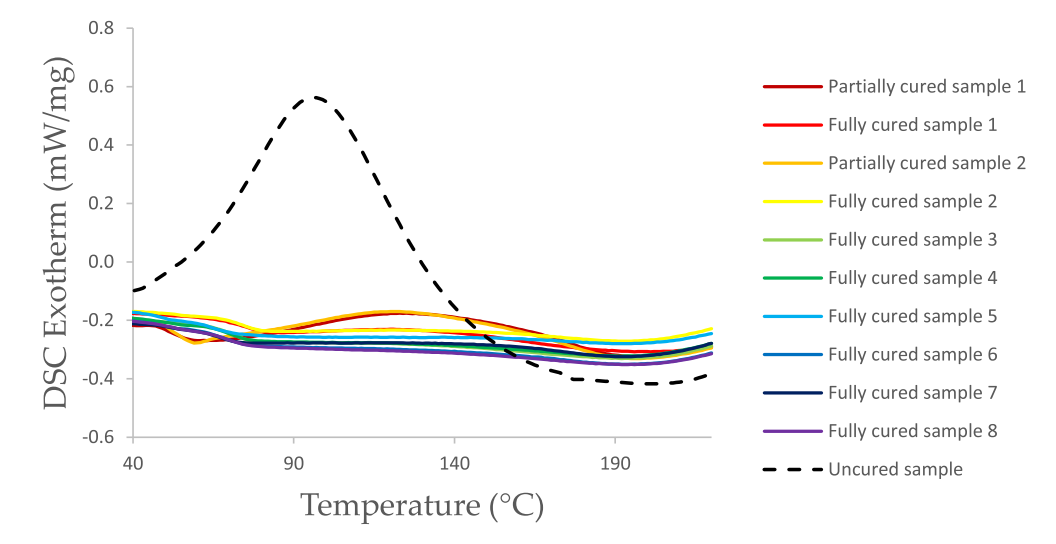
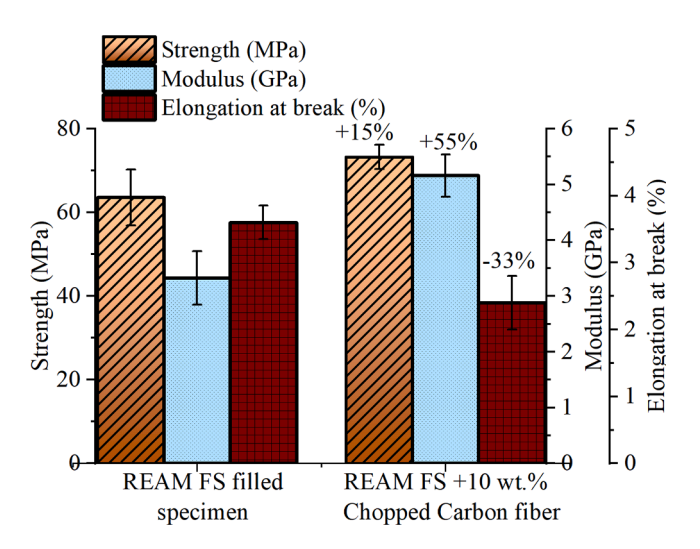


Fig. 8. DSC curves for samples taken from the racetrack part. The dashed curve is a separately prepared control sample that represents the curing cycle.



rasters with greater shape retention. While this outcome has obvious benefits in reducing slumping, it would also be beneficial for more complicated tasks, such as bridging or overhangs. The observed cure characteristics (>94 % cured) in resulting fiber reinforced samples also showed that no post-treatment is needed. The material property

improvements, particularly the large stiffness increase and mild tensile strength increase (55 % and 15 %, respectively) relative to unfilled epoxy, were consistent with known trends in short fiber composites and indicative of fibers below the critical length. Additionally, modeling results underscored the importance of mean fiber length for achieving higher strength. Increasing the fiber content led to a reduction in length when mixed with the resin. The balance between a higher volume ratio and reduced length determines the best fiber fraction for maximizing strength. Concurrently, as the fiber volume fraction goes up, the modulus also increases.

5. Future work

Although this study represents a substantial step forward in developing the capabilities of REAM, there are numerous avenues for improvement. The mixing time adopted in this study was too long, which degraded fiber lengths below the critical value necessary for more substantial strength enhancement. Future work should delineate the tradeoff between mixing time and various practical considerations (fiber volume fraction, final fiber length, and ease of pumping). Although far less fiber breakdown in the active mixing element (~20 s mixing time) is anticipated compared to pre-mixing steps (>1 h mixing time), breakdown in the active mixing element should still be quantified with computed tomography. There was also no significant fiber alignment found in the samples, which could be improved through faster deposition speeds or smaller nozzle diameters [34]. Instead of a heated, metal print bed, an insulating print bed should be used to drive complete cure

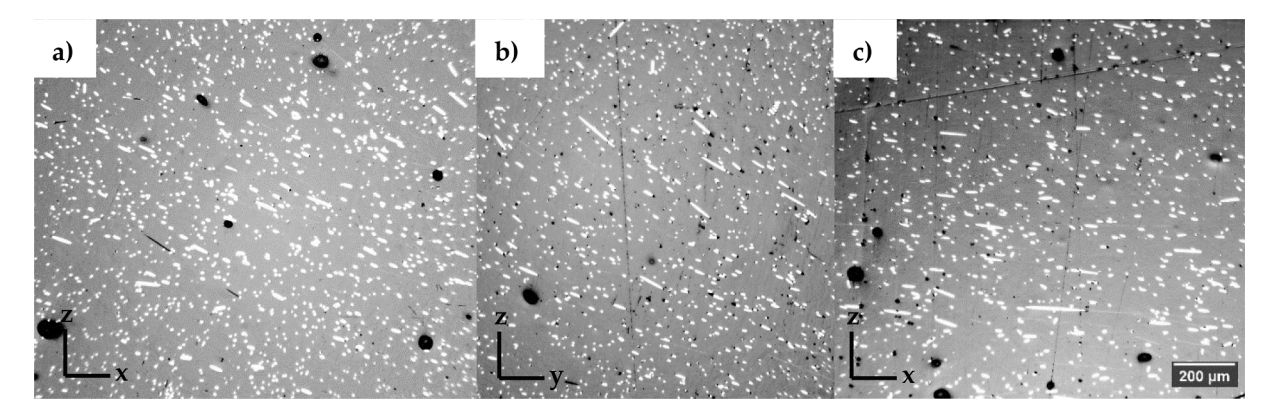


Fig. 10. Representative cross sections of an actively mixed REAM part showing random fiber alignment. a and b are from the middle, c is from the top, and b is in the normal plane. The coordinates shown here match those in Fig. 6. No significant alignment was seen in any recorded micrographs.

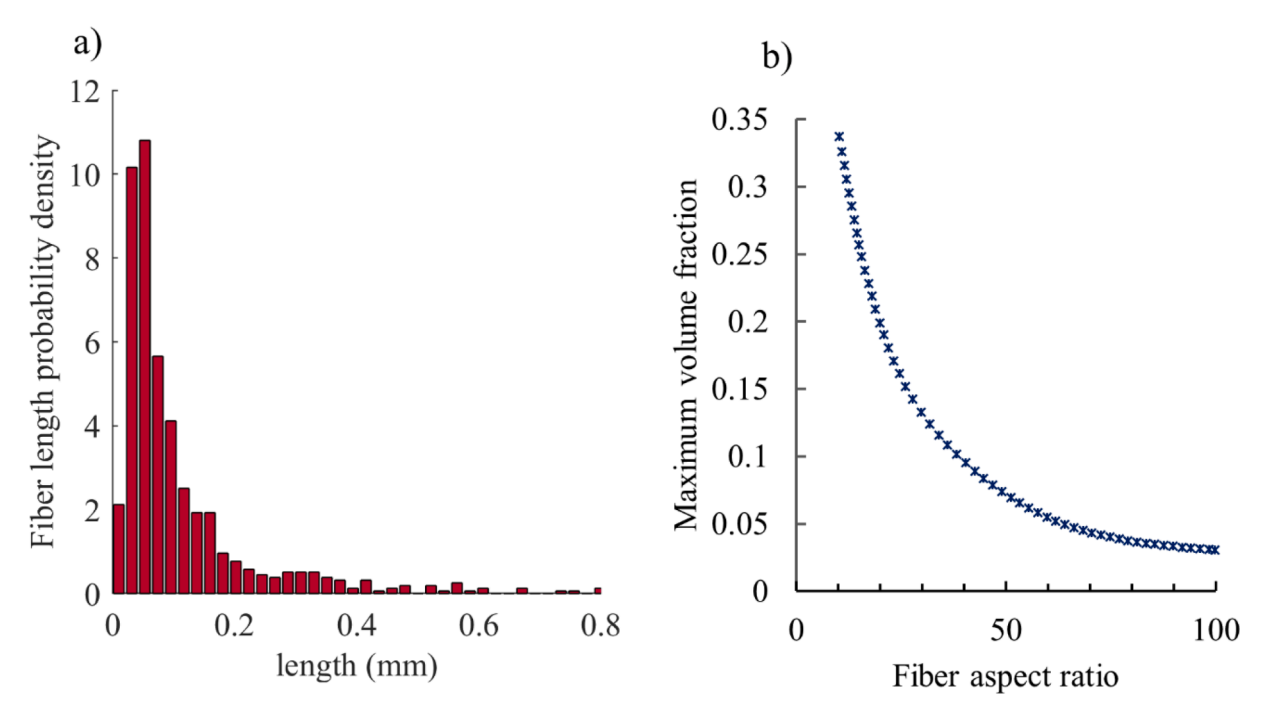


Fig. 11. a) Fiber length probability for the 10 wt.% carbon fiber in resin. b) Maximum achievable fiber volume fraction versus fiber aspect ratio in a composite [33].

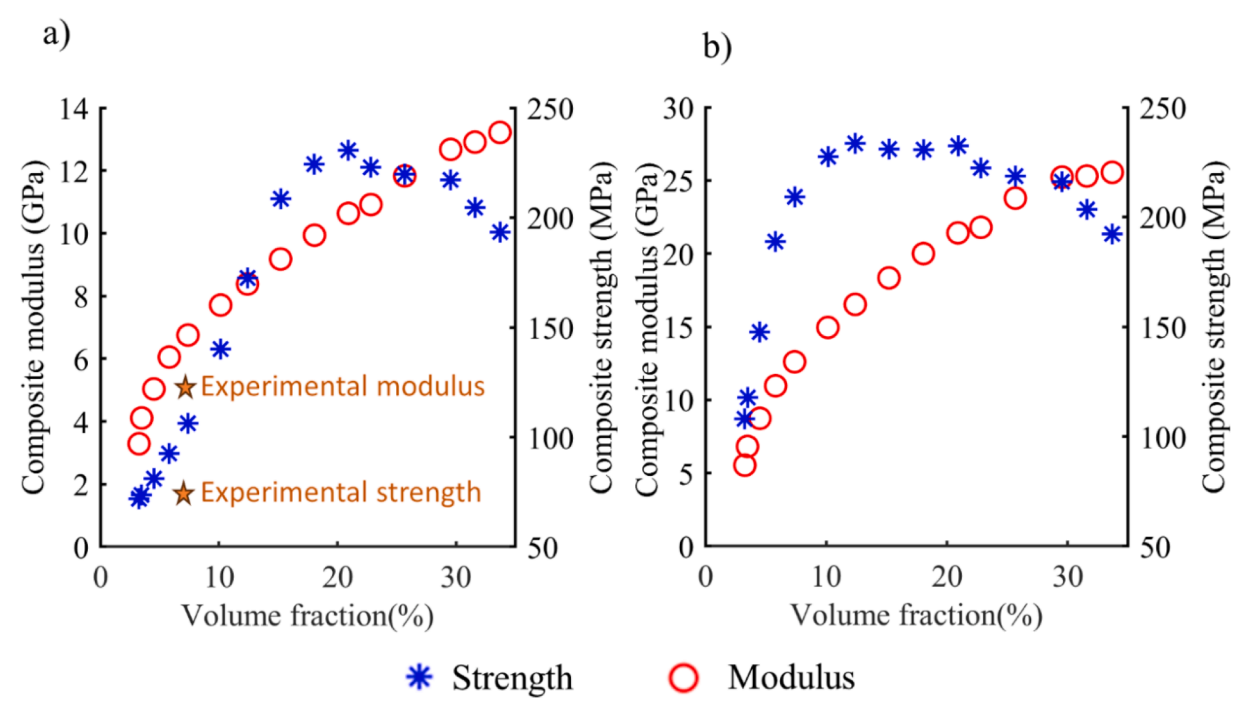


Fig. 12. Composite tensile strength and modulus as a function of fiber volume fraction (considering the effect of fiber shortening due to mixing at high volume fractions) and the aspect ratio of fiber for a) randomly and b) aligned fiber distributions.

of bottom layers, while taking care not to thermally degrade the bottom section. This work developed single-use mixing elements, which was useful for rapid prototyping, but should be expanded into a multi-use system to reduce material waste and stay in line with REAM's advantages of sustainability. The "scoop test" employed in this study likely has inherent variability from the initial velocity of any sample dropped onto a surface, so this qualitative test ought to be substituted with a quantitative test akin to the concrete "slump test" [36]. Finally, an extensive analysis of factors involved in geometrical fidelity of REAM should be established.

CRediT authorship contribution statement

Pratik Koirala: Conceptualization, Data curation, Formal analysis, Investigation, Writing – original draft, Writing – review & editing, Visualization. **Robert Pavlovic:** Conceptualization, Data curation, Formal analysis, Investigation, Methodology, Visualization, Writing – original draft, Writing – review & editing. **Athena Aber:** Conceptualization, Formal analysis, Investigation, Writing – review & editing. **Michael J. Fogg:** Data curation, Investigation, Writing – review & editing. **Cole Mensch:** Investigation, Writing – original draft. **Carolyn**

C. Seepersad: Conceptualization, Funding acquisition, Investigation, Methodology, Project administration, Supervision, Writing – review & editing. **Mehran Tehrani:** Conceptualization, Funding acquisition, Investigation, Methodology, Project administration, Supervision, Writing – review & editing.

Declaration of competing interest

The authors declare that they have no known competing financial interests or personal relationships that could have appeared to influence the work reported in this paper.

Data availability

Data will be made available on request.

Acknowledgments

The authors would like to acknowledge the National Science Foundation (NSF) awards CMMI-1953259, CMMI-2401218, and CMMI-2152984, Lockheed Martin (LHM), and the Air Force Office of Scientific Research (AFOSR) award #FA9550-21-1-0066 for their support of this research.

Appendix A. Supplementary data

Supplementary data to this article can be found online at https://doi.org/10.1016/j.compositesa.2023.107989.

References

- [1] Mahshid R, Isfahani MN, Heidari-Rarani M, Mirkhalaf M. Recent advances in development of additively manufactured thermosets and fiber reinforced thermosetting composites: technologies, materials, and mechanical properties. Compos A Appl Sci Manuf 2023:107584.
- [2] Stenzenberger H. Recent developments of thermosetting polymers for advanced composites. Compos Struct 1993;24(3):219–31.
- [3] Tamez MBA, Taha I. A review of additive manufacturing technologies and markets for thermosetting resins and their potential for carbon fiber integration. Addit Manuf 2021;37:101748.
- [4] O. L. Uitz, "Reactive Extrusion Additive Manufacturing (REAM) with applications to magnetically actuated shape memory thermoset composites," 2021.
- [5] Koirala P, Uitz OL, Oridate AA, Seepersad CC, Tehrani M. Reactive Extrusion Additive Manufacturing of a Short Fiber Reinforced Thermoset Composite. in Proceedings of the American Society for Composites—Thirty-Sixth Technical Conference on Composite Materials. 2021.
- [6] J. Lindahl et al., "Large-scale additive manufacturing with reactive polymers," Oak Ridge National Lab.(ORNL), Oak Ridge, TN (United States), 2018.
- [7] Rios O, et al. 3D printing via ambient reactive extrusion. Mater Today Commun 2018;15:333–6.
- [8] Uitz OL, Koirala P, Tehrani M, Seepersad CC. Fast, low-energy additive manufacturing of isotropic parts via reactive extrusion. Addit Manuf 2021;41: 101919.
- [9] S. Romberg, C. Hershey, J. Lindahl, W. Carter, B. G. Compton, and V. Kunc, "Large-scale additive manufacturing of highly exothermic reactive polymer systems," Oak Ridge National Lab.(ORNL), Oak Ridge, TN (United States), 2019.
- [10] Duty C, et al. What makes a material printable? A viscoelastic model for extrusion-based 3D printing of polymers. J Manuf Process 2018;35:526–37.
- [11] Romberg SK, et al. Linking thermoset ink rheology to the stability of 3D-printed structures. Addit Manuf 2021;37:101621.
- [12] C. Hershey et al., "Large-scale reactive extrusion deposition of sparse infill structures with solid perimeters," Oak Ridge National Lab.(ORNL), Oak Ridge, TN (United States), 2019.

- [13] Sarmah A, et al. Additive manufacturing of nanotube-loaded thermosets via direct ink writing and radio-frequency heating and curing. Carbon 2022;200:307–16. https://doi.org/10.1016/j.carbon.2022.08.063.
- [14] M. A. S. R. Saadi et al., "Direct ink writing: a 3D printing technology for diverse materials," Adv Mater (Weinheim), vol. 34, no. 28, pp. e2108855-n/a, 2022, doi: 10.1002/adma.202108855.
- [15] Robertson ID, et al. Rapid energy-efficient manufacturing of polymers and composites via frontal polymerization. Nature (London) 2018;557(7704):223–7. https://doi.org/10.1038/s41586-018-0054-x.
- [16] F. Fernandez, W. S. Compel, J. P. Lewicki, and D. A. Tortorelli, "Optimal design of fiber reinforced composite structures and their direct ink write fabrication," *Comput Methods Appl Mech Eng*, vol. 353, no. C, pp. 277-307, 2019, doi: 10.1016/j. cma.2019.05.010.
- [17] Nawafleh N, Celik E. Additive manufacturing of short fiber reinforced thermoset composites with unprecedented mechanical performance. Addit Manuf 2020;33: 101109
- [18] Nguyen DT, et al. 3D printing of compositional gradients using the microfluidic circuit analogy. Adv Mater Technol 2019;4(12):1900784.
- [19] W. Li et al., "Fabricating functionally graded materials by ceramic on-demand extrusion with dynamic mixing," in 2018 International Solid Freeform Fabrication Symposium, 2018: University of Texas at Austin.
- [20] Ober TJ, Foresti D, Lewis JA. Active mixing of complex fluids at the microscale. Proc Natl Acad Sci 2015;112(40):12293–8.
- [21] B. Newman, C. Creighton, L. C. Henderson, and F. Stojcevski, "A review of milled carbon fibres in composite materials," *Compos Part A: Appl Sci Manuf*, p. 107249, 2022
- [22] Guo F-L, et al. Modeling and characterizations of mechanical behaviors of short carbon fiber and short glass fiber reinforced polyetherimide composites. Compos Sci Technol 2022;229:109685.
- [23] A. Obeng, V. Penny, and W. Armenante, "Handbook of industrial mixing: Science and practice," ed: Hoboken, NJ: Wiley-Interscience, 2004.
- [24] Koirala P, Uitz OL, Tehrani M. Printability of highly viscous composite slurries via reactive extrusion additive manufacturing. in Proceedings of the American Society for Composites—Thirty-fifth Technical Conference. 2020.
- [25] Fu S-Y, Lauke B. Effects of fiber length and fiber orientation distributions on the tensile strength of short-fiber-reinforced polymers. Compos Sci Technol 1996;56 (10):1179–90.
- [26] Van de Werken N, Reese MS, Taha MR, Tehrani M. Investigating the effects of fiber surface treatment and alignment on mechanical properties of recycled carbon fiber composites. Compos A Appl Sci Manuf 2019;119:38–47.
- [27] Fu S-Y, Lauke B. The elastic modulus of misaligned short-fiber-reinforced polymers. Compos Sci Technol 1998;58(3–4):389–400.
- [28] Rau DA, Bortner MJ, Williams CB. A rheology roadmap for evaluating the printability of material extrusion inks. Addit Manuf 2023:75:103745.
- [29] Hexion. Technical Data Sheet EPON™ Resin 8111 [Online] Available: https://www.hexion.com/CustomServices/PDFDownloader.aspx? type=tds&pid=53e3d33b-5814-6fe3-ae8a-ff0300fcd525.
- [30] Jones DAR, Leary B, Boger DV. The rheology of a concentrated colloidal suspension of hard spheres. J Colloid Interface Sci 1991;147(2):479–95. https://doi.org/ 10.1016/0021-9797(91)90182-8.
- [31] Khatri NR, Islam MN, Cao P-F, Advincula RC, Choi W, Jiang Y. Integrating helicoid channels for passive control of fiber alignment in direct-write 3D printing. Addit Manuf 2021:48:102419
- [32] B. Heller, D. E. Smith, and D. A. Jack, "Effect of extrudate swell, nozzle shape, and convergence zone on fiber orientation in fused deposition modeling nozzle flow," in 2015 International Solid Freeform Fabrication Symposium, 2015: University of Texas at Austin.
- [33] Von Turkovich R, Erwin L. Fiber fracture in reinforced thermoplastic processing. Polym Eng Sci 1983;23(13):743–9.
- [34] Hmeidat NS, Elkins DS, Peter HR, Kumar V, Compton BG. Processing and mechanical characterization of short carbon fiber-reinforced epoxy composites for material extrusion additive manufacturing. Compos B Eng 2021;223:109122.
- [35] van de Werken N, Tekinalp H, Khanbolouki P, Ozcan S, Williams A, Tehrani M. Additively manufactured carbon fiber-reinforced composites: State of the art and perspective. Addit Manuf 2020;31:100962. https://doi.org/10.1016/j. addma.2019.100962.
- [36] Tuan NM, Hau QV, Chin S, Park S. In-situ concrete slump test incorporating deep learning and stereo vision. Autom Constr 2021;121:103432. https://doi.org/ 10.1016/j.autcon.2020.103432.